Egyptian Journal of Pure and Applied Science

Sorption Behavior of some Lanthanides on Graphene Oxide-Manganese dioxide Composite

Zakaria A. Mekawy[1*], Reda R. Sheha[1], Hanan H. Someda[1], Mohamed K. K. Shehata[1] and Wagiha H. Mahmoud[2]

[1] *Nuclear Chemistry Department, Hot Lab. Center, Atomic Energy Authority, P.O. 13759, Cairo, Egypt*
[2] *Department of Chemistry, Faculty of Science, Ain Shams University, Cairo, Egypt*

ARTICLE INFO

Article history:
Received 02 July 2019
Accepted 26 August 2019

Keywords:
Synthesis;
GO-MnO_2 composite;
Eu(III);
Ce(III);
Sorption kinetics;
Desorption studies.

ABSTRACT

In this study, Manganese dioxide decorated graphene oxide (GO-MnO_2 composite) was prepared via fixation of MnO_2 on the surface of graphene oxide (GO) and used as an adsorbent for separation of europium and cerium ions from aqueous solutions. GO, MnO_2 and GO-MnO_2 composite were characterized using scanning electron microscope (SEM), Thermal analysis (TGA), X-ray diffraction (XRD), Raman spectroscopy and Fourier transform infrared spectrum (FT-IR). The role of different variable as: contact time, solution pH, metal ion concentration, adsorbent dosage, ionic strength and temperature on sorption efficiency was studied using batch technique. It was found that sorption of Eu(III) and Ce(III) ions on synthesized adsorbents could be described more favorably by pseudo-second-order kinetic model. Sorption data have been interpreted in terms of both Freundlich and Langmuir isotherms. Desorption of Eu(III) and Ce(III) ions from loaded samples was studied using different eluents. The data suggest the possible use of synthesized sorbents for separation of these lanthanides from their aqueous solutions.

Introduction

Lanthanide elements enter environment through different pathways as a result of the rapid increase in their usage in several fields of modern industry, as well as a variety of applications in nuclear fields [1]. As a representative member of lanthanides, europium typically appears in the oxidation state +3 and in some cases the oxidation state +2 [2]. The radioisotopes of europium are used as burn up monitors to evaluate the performance and characteristics of reactors fuels [3]. $^{152+154}$Eu is one of the most hazardous contaminants presents in radioactive wastewaters due to its relatively high energy (hard γ-emitter) and long half-life (13.54 and 8.5 y).

Cerium is one of the rare earth elements (REEs) which is used extensively in chemical processes, luminescence, catalysis, nuclear energy, metallurgy, microelectronics, and therapeutic applications [4]. Cerium, like other REEs, is considered to be toxic, but its toxicity is in low to-moderate range [5].

Various methods such as selective precipitation, ion exchange [6], solvent extraction [7], membrane filtration [8] and adsorption [9] have been employed for separation of different lanthanide elements from aqueous solutions. Sorption approach is widely used in treatment of rare earth elements-bearing solutions due to its multiple superiorities of easy operation, low cost, high availability and favorable removal performance [10].

Various materials like zeolite, clay minerals, polymeric materials, iron oxide nanomaterials, and activated carbons, etc. were commonly used as adsorbents for these lanthanide elements [11]. However, many of these materials encountered some drawbacks that limit their application in practice, such as low adsorption capacity, low efficiencies and separation inconvenience [12]. Therefore, it is necessary to develop novel sorbents to overcome these disadvantages.

Graphene is a kind of typical quasi two-dimensional laminar carbon material. Graphene oxide (GO), the oxidized form of graphene, is one of the most important graphene-based materials that holds many oxygen functional groups such as epoxy, hydroxyl and carboxylic groups between the lamellas. GO exhibits high sorption capacity for removal of heavy metal ions, cationic dyes and organic pollution from aqueous solution [13]. Zhao *et al.* [14] prepared few-layered graphene oxide (FGO) and proved that FGO exhibits higher sorption capacity for Pb(II).

* Corresponding author.
E-mail address: zakaria.chemist@gmail.com

Manganese (Mn) is one of the most abundant elements in Earth's crust that easily oxidized to various Mn oxide/hydroxides as α-MnO_2, δ-MnO_2, β-MnO_2, α-MnOOH, δ-MnOOH, and γ-MnOOH. Manganese dioxide (MnO_2) is one of the most stable manganese oxides which have excellent physical and chemical properties under ambient conditions [15]. These Mn oxides/hydroxides play important roles in the fate and transport of heavy metal ions and/or radionuclides in the natural water and soil environment. They were used to pre-concentrate some naturally occurring radioisotopes from their natural sources [16]. In addition, Warwick *et al.* [17] studied the sorption of Eu(III) by MnO_2 and observed quantitative sorption at all pH values. Combining MnO_2 with carbon based materials such as graphene oxide can improve its physico-chemical properties [18]. Hence, many investigations were carried out on synthesis of GO-MnO_2 composite and applying it as sorbent for separation of different metal ions from aqueous solutions [19].

The objective of the presented work is to investigate the preparation a new and effective sorbent such as: GO, MnO_2 and GO-MnO_2 composite for sorption of $^{152+154}$Eu and ^{141}Ce from their aqueous solutions. The effects of pH, contact time, initial metal concentration and temperature on Eu(III) and Ce(III) sorption onto synthesized sorbents were studied. Adsorption kinetics, isotherms and thermodynamic parameters were also evaluated and reported.

Subjects and Methods

Chemicals and Reagents

All chemicals used were of analytical grade purity and were used without further purification. Graphite (fine powder extra pure) was purchased from Merck Co., Germany. A stock solution of 1000 mg L^{-1} Eu(III) ions was prepared by dissolving the required amount of europium oxide in a definite volume of concentrated hydrochloric acid and re-dissolved in double distilled water to obtain a clear solution. While Ce(III) ions were prepared by dissolving the required amount of cerium oxide in a definite volume of a mixture of HNO_3 and H_2O_2 (1:1 ratio by volume), and re-dissolved in double distilled water to obtain a clear solution.

Synthesis of Graphene Oxide (GO)

Graphene oxide (GO) was synthesized according to the modified Hummers method [20]. In detail, 69 ml of concentrated H_2SO_4 (98 %) was added to a mixture of graphite (1.5 g) and $NaNO_3$ (1.5 g) with continuously stirring in ice bath until a uniform paste was formed. After that, $KMnO_4$ (9.0 g) was added gradually to the above paste while keeping the temperature less than 20°C to prevent overheating and explosion. The mixture was removed from ice bath and stirred at room temperature for 2 h. The color of the suspension would become bright brown. Then, 90 ml of distilled water was added. The temperature of the suspension would reach quickly to 98°C and the color would change to yellow. The diluted suspension was stirred at 98°C for 12 h and 30 ml of 30 % H_2O_2 was added to the mixture to ensure the completion of reaction with $KMnO_4$. The suspension was then filtered and washed several times with distilled water. After that, the suspension was centrifuged at 4000 rpm for 6 min. To fully exfoliate GO sheets, the resulting solution was sonicated using a tabletop ultrasonication cleaner for 1 h. After that, the remaining solid material was dried at 80°C for 24 h.

Synthesis of manganese dioxide (MnO_2)

Manganese oxide was prepared by dissolving 0.5 g of $KMnO_4$ was dissolved in 30 ml of bi-distilled water. To this solution, 10 ml of ethanol was added drop-wise where brownish precipitate of MnO_2 was formed according to the following reaction:

$$4KMnO_4 + 3CH_3CH_2OH \rightarrow 3CH_3COOK + 4MnO_2 + KOH + 4H_2O$$

The precipitate was filtered and washed extensively with bi-distilled water until pH of the water is 7. Then, the precipitate was dried at 100°C [21].

Synthesis of GO-MnO_2 composite

GO-MnO_2 composite was synthesized by mixing of GO with MnO_2 on a weight ratio of 5:1. A black-brown powder, with uniform color, was obtained. The obtained powder was immersed in bi-distilled water and irradiated with ultrasonic waves for 1 h. No additional washing was needed and the final yield was denoted as GO–MnO_2 [22].

Preparation of radioisotopes

$^{152+154}$Eu and ^{141}Ce isotopes were produced by neutron irradiation using the Egyptian Research Reactor ARE-RR-2 at Inshas, Egypt. An accurate weight of europium and cerium oxides were separately wrapped in a thin high purity aluminum foil and placed in a thick aluminum irradiation capsule which was then subjected to pile neutrons in the reactor. The irradiated targets were left for a period of time to cool. After cooling, the irradiated europium oxide was dissolved in a minimum volume of concentrated hydrochloric acid. While cerium oxide was dissolved in a mixture of HNO_3 and H_2O_2 (1:1 ratio). After complete dissolvation, the solutions were heated to dryer, then redissolved in bi-distilled water. The prepared isotopes were used as tracers in equilibrium and kinetic measurements. The radioactivity of the prepared isotopes was γ-radiometrically assayed using a single channel analyzer supplied with a well type NaI (Tl) detector.

Characterization methods

The morphology of the synthesized sorbents was depicted using Jeol scanning electron microscope, model JSM-6510A from Japan. The system operates with primary beams have electrons ranged from 5 to 30 keV. Fourier transformer infrared (FT-IR) of type Nicolet is10 spectrometer from Meslo, (USA) was used to analyze the surface functionality of prepared samples using disc technique. The sample was thoroughly mixed with KBr as a matrix. The spectrum was recorded at a wavelength of 400–4000 cm^{-1}. X-ray diffraction of Model XRD 490, Japan, was employed to determine the

crystalline phase. The scanning was measured at values of 2θ in the range from 10 to 80°, using a CuK_α radiation of an incident beam (λ = 0.15406 nm) monochromator. Shimadzu TGA-DTA system of type TGA-DTA-50, Japan, was used for measuring the weight loss and phase changes of samples, respectively. The heating rate was 10°C min^{-1} in presence of nitrogen gas to avoid thermal oxidation of sample. Raman analysis was carried out using a Horiba Jobin Yvon HR 800UV with a 532 nm He–Ne laser as a light source. MICROMERITICS GEMINE 2375 surface area analyzer, (USA), was used for measuring the specific surface area of the synthesized sorbents using the standard adsorption of N_2 gas.

Sorption experiments

The sorption experiments were carried out using batch technique. The experiments were performed by contacting 0.01 g of the synthesized sorbents and 5 ml solution of europium or cerium ions have 50 mg. L^{-1} initial concentration and traced with $^{152+154}Eu$ or ^{141}Ce radionuclides in sealed glass bottle. The mixtures were stirred at room temperature (25 ± 1°C) for 2 h using a flask shaker (SF1, stuart scientific, UK).

After equilibrium, sorbents were separated by centrifugation and supernatants were subjected to γ-radio assay. The activity of supernatants was measured using a single channel analyzer supplied with a well-type NaI(Tl) detector. To explore the role of different experimental parameters, numbers of experiments were carried at different conditions. For pH experiments, the initial pH was varied between 2 and 7 and the values were adjusted using solutions of NaOH and/or HCl. Also, samples were taken at different time periods ranged from 5 min to 48 h to determine the time at which sorption equilibrium was attained. The sorbent dosage was varied in the range 0.005 - 0.1 g. Sorption of studied lanthanides was carried out at different initial concentrations ranged from 25 to 300 mg. L^{-1}. A set of sorption experiments were also carried out at 20, 30, 40, 50 and 60°C to determine the sorption thermodynamic parameters. The uptake percent in our investigations were determined according to:

Uptake percentage (U%) =

$$(C_o-C_e)/C_o \times 100 \quad (1)$$

where: C_o is the initial concentration and C_e is the concentration at equilibrium.

The adsorbed amount of metal ions was calculated as follows:

$$q_e = (C_o - C_e) \times V/m \quad (2)$$

where: q_e is the amount of metals ions adsorbed by the synthesized sorbents ($mg.g^{-1}$), V is the initial solution volume (L) and m is the sorbent dose (g).

Results and Discussion

Characterization

The synthesized GO, MnO_2 and GO-MnO_2 composite were characterized using different techniques as using FTIR spectroscopy, scanning electron microscope, thermal analysis, X-ray diffraction, and Raman spectroscopy and revealed data are discussed below.

FT-IR analysis

The IR spectra of GO, MnO_2 and GO-MnO_2 composite are presented in **Fig. 1**. The spectra show bands at 3400 cm^{-1} could be assigned to the hydroxylic group of moisture, or carboxylic groups on the surface of the synthesized sorbents [23]. The peaks detected around 2925-2851cm^{-1} may due to asymmetric and symmetric C–H stretching vibrations in aliphatic –CH originating from the surface of GO sheets [24]. The bands revealed at 1730, 1620 and 1400 cm^{-1} could be attributed to the stretching vibrations of carbonyl groups C=O, C=C and carboxyl =C–O groups, respectively. The band observed at 1335 cm^{-1} may be ascribed to bending vibration of the hydroxyl group of COOH. The peak exhibited at 1035 cm^{-1} may due to stretching vibration of epoxy –C–O group [25]. It is indicated that abundant oxygen containing functional groups exist on the surface of GO sheets GO-MnO_2 composite [26]. The IR spectrum of MnO_2 in **Fig. 1b** show peak at 1625 cm^{-1} is due to the O–H bending vibration [27], the peaks at 509 and 460 cm^{-1} are referred to Mn–O vibration [26]. Compared with **Fig. 1b, Fig. 1c** shows an additional sharp peak around 510 cm^{-1} which can be attributed to the Mn–O and Mn–O–Mn vibration of MnO_2 [28]. So, the FT-IR spectrum reveals that MnO_2 particles were decorates the GO sheets.

SEM study

Fig. 2 shows the SEM images of GO, MnO_2 and GO–MnO_2 composite. MnO_2 image exhibited almost spherical morphology with large aggregates and a typical flower structure of MnO_2 with rough agglomeration [19]. GO and GO–MnO_2 exhibited similar lamellar wrinkled structures and MnO_2 ultrathin flakes are loosely assembled and closely anchored on both sides of GO sheet, representing a multilayer flake structure, but the sheets of GO stacked together due to its strong inter-planar interactions and GO sheets have been exfoliated and decorated randomly with structure the MnO_2 [19, 29].

Surface area measurements

Surface area and porosity are two important physical properties that impact the quality and utility of any adsorbent material. The Brunauer, Emmett and Teller (BET) technique is the most common method for determining the surface area of powders and porous materials of any solid sorbent. Nitrogen gas adsorption and desorption isotherms were applied in measuring the surface area and pore volume of synthesized sorbents and the corresponding results are listed in **Table 1**. BET surface area was determined by a multipoint BET method using the adsorption data in relative pressure (P/P_o) ranged from 0.05 to 1.09. The nitrogen adsorption volume at the relative pressure (P/P_o) of 0.9865 was used to determine the pore volume and average pore size for synthesized samples.

According to BET method, the synthesized sorbents have specific surface area of 34.27, 18.09 and 45.74 $m^2.g^{-1}$ for GO, MnO_2 and GO–MnO_2, respectively. The total pore volume attains the values 0.03, 0.02 and 0.05

$cm^3.g^{-1}$ for GO, MnO_2 and GO-MnO_2, while their pore diameters have the values 1.61, 2.11and 3.91 nm, respectively. It is obvious from these data that the GO–MnO_2 composite have higher values of S_{BET}, V_P and D_P compared with that of their precursors GO and MnO_2. These properties declare the promising surface characteristics of the GO-MnO_2 composite to be used as novel sorbent for removal of different metal ions from aqueous solution.

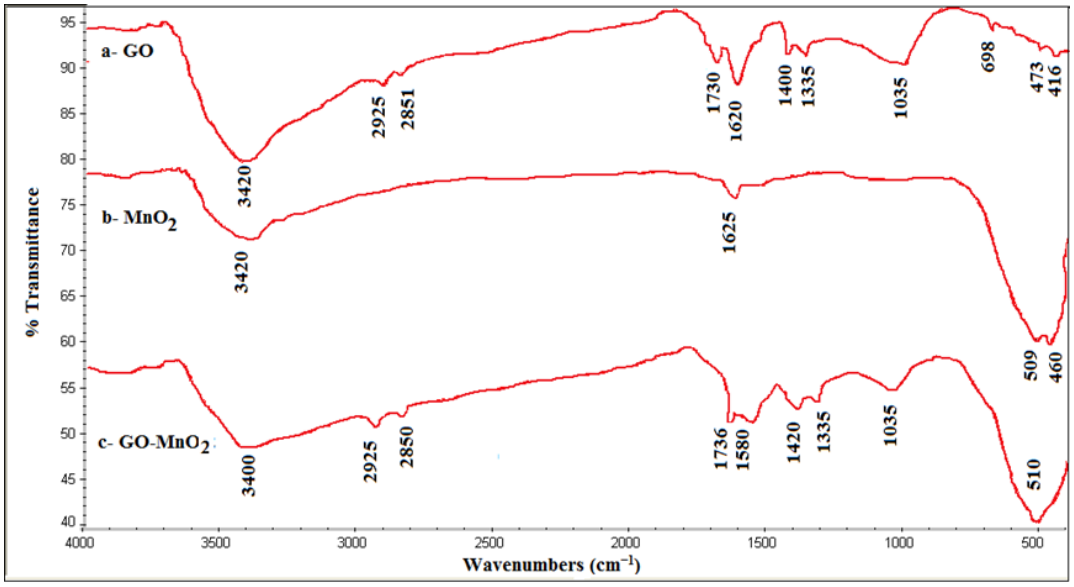

Fig. 1: The FT-IR spectrum of the synthesized (a) GO, (b) MnO_2 and (c) GO–MnO_2 composite.

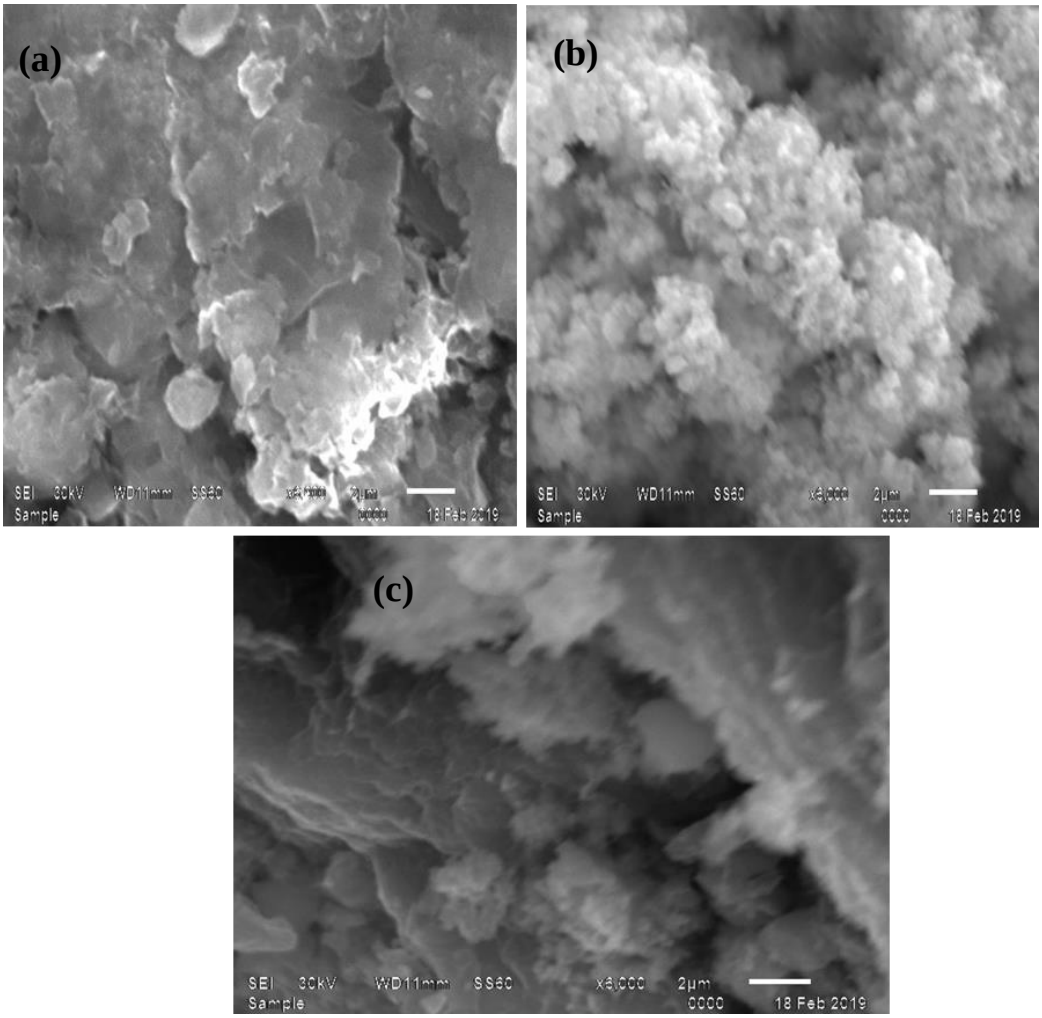

Fig. 2: SEM images of the synthesized (a) GO, (b) MnO_2 and (c) GO–MnO_2 composite.

Table 1: Surface area parameters of the synthesized sorbents

Sorbents	Surface area parameters		
	S_{BET} ($m^2 . g^{-1}$)	V_P ($cm^3 . g^{-1}$)	D_P (nm)
GO	34.27	0.03	1.61
MnO_2	18.09	0.02	2.11
GO–MnO_2	45.74	0.05	3.91

Thermal analysis

The thermal stability of GO, MnO_2 and GO-MnO_2 composite was studied using TGA and data are shown in **Fig. 3**. The thermograms of GO is represented in **Fig. 3a.** The figure shows two distinct weight losses were observed on the TGA profile of GO. An initial weight loss was observed with rising temperature up to 170°C. GO exhibited a loss in weight amounted to 13.98 %. This loss could be attributed to the removal of physically adsorbed water molecules [30]. The gradual weight decreases in a temperature range of 170–250°C could be attributed to the removal of the residual oxygenate groups, such as hydroxyl, carboxyl, and carbonyl groups on the surface of GO and the loss of interlayer water molecules. This weight loss was amounted to ~ 67.91 %. In the temperature range of 250−-630°C the weight loss was amounted to ~ 14.48 %. This could be attributed to the burning of carbon sketch of GO. The thermal analysis of the MnO_2 particles is shown in **Fig. 3b**. MnO_2 particles shows two major weight losses between 50 and 800°C. The first weight loss (about 13.33 %) was revealed below 200°C and could be attributed to removal of physically adsorbed water molecules and dehydration of MnO_2. The second small weight loss (about 6.56 %) occurred between 200 and 800°C and could be attributed to the loss of lattice oxygen species corresponding to the reduction of tetravalent manganese [31].

It is clear that MnO_2 particles are stable within the temperature between 25 to 800°C. The result of TG analysis of the GO–MnO_2 composite is shown in **Fig. 3c**. A weight loss amount to 11.19 % was detected below 200°C. This weight loss could be attributed to the removal of surface-adsorbed water. Another weight loss was observed at temperature ranged from 190 to 300°C. This weight loss was amounted to 4.05 % and could be attributed to the removal of interlayer water molecules impeded in lattice structure [32]. In addition, the composite suffered from an additional loss in its weight with rising temperature from 300-800°C. This weight loss was amounted to 37.63 % and could be revealed to the decomposition of carbon sketch through burning of GO [32]. From TGA analysis, it can conclude that, addition of MnO_2 to GO improves thermal stability of GO.

X-ray diffraction

The XRD measurements of graphite, GO, MnO_2 and GO–MnO_2 composite are exhibited in **Fig. 4**. The obtained diffractogram of graphite powder is given in **Fig.4a.** This figure shows a very sharp diffraction peak at $2\theta = 26.6°$ corresponding to the diffraction of (002) plane and a diffraction peak at $2\theta = 53.5°$ corresponding to the diffraction of (004) plane (JCPDS card no. 8-415). These peaks are characteristic to the graphite powder [33]. GO shows a strong and sharp diffraction peak at about $2\theta = 10.6°$ corresponds to the (001) reflection plane of stacked GO sheets as shown in **Fig. 4b.** Also, a peak detected at $2\theta = 43°$ that might be attributed to the (100) crystal plane of graphene oxide. MnO_2 particles exhibit four broad diffraction peaks could be identified as (001), (002), (200) and (310) diffractions for the birnessite MnO_2 structure (JCPDF 43-1456) [34] as shown in **Fig. 4c** It is important to note that the (001) diffraction peak at $2\theta \sim 12.2°$ (for MnO_2 birnessite) and (002) at $2\theta \sim 25°$ is a fingerprint of this layered MnO_2 allotrope. Also, (200) and (310) diffraction peaks at $2\theta \sim 37°$ and $2\theta \sim 66$ ° are commonly observed in manganese oxide diffraction patterns [34, 35]. Finally, GO–MnO_2 composite, the (001) reflection peak of layered GO has almost weaken as shown in **Fig. 4d**. This result correlated with the report that the diffraction peaks of MnO_2 become weakened or even disappears whenever the regular stacks of GO are exfoliated [36].

Raman spectroscopy

The Raman spectra of synthesized GO and GO–MnO_2 composite are recorded in **Fig. 5a&b.** The figure clarifies Raman band at 1584 cm^{-1} for GO which is denoted as G band (Graphite band). It was related to the C–C bond vibration of the carbon material with a sp^2 orbital structure [37]. This band was shifted to 1597 cm^{-1} in GO–MnO_2 composite, **fig. 5b**. The Raman band appeared at 1338cm^{-1} was denoted as D band (Disorder band) for GO and GO–MnO_2 composite, respectively. This band could be attributed to the disorder-induced vibration of C–C bond in the graphitic layers [38]. The Raman band appeared at ~ 630 cm^{-1} could be referred to Mn–O vibration in GO–MnO_2 composite. This band confirms the formation of a composite between GO and MnO_2 particles [39].

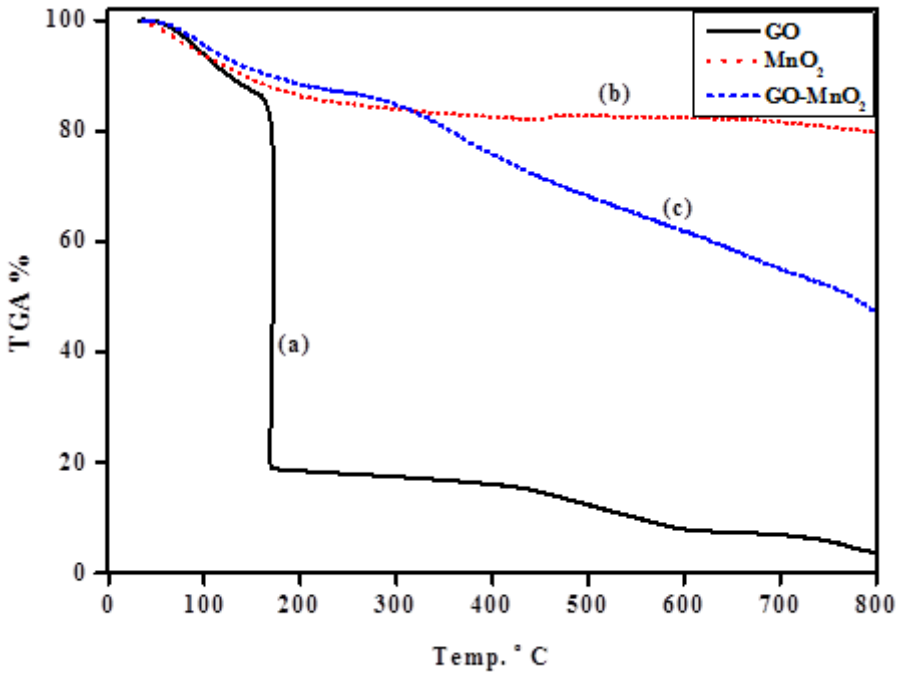

Fig. 3: Thermogravimetric (TGA) of the synthesized (a) GO, (b) MnO_2 and (c) GO-MnO_2 composite.

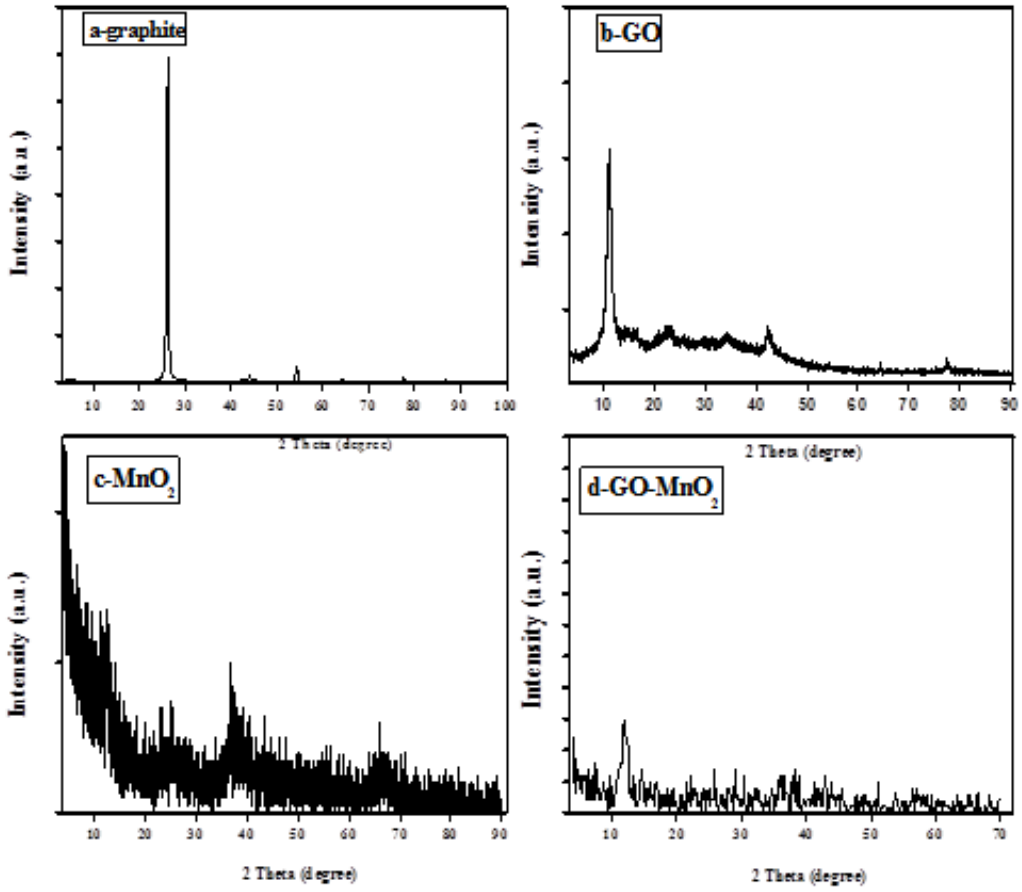

Fig. 4: XRD patterns of the synthesized samples.

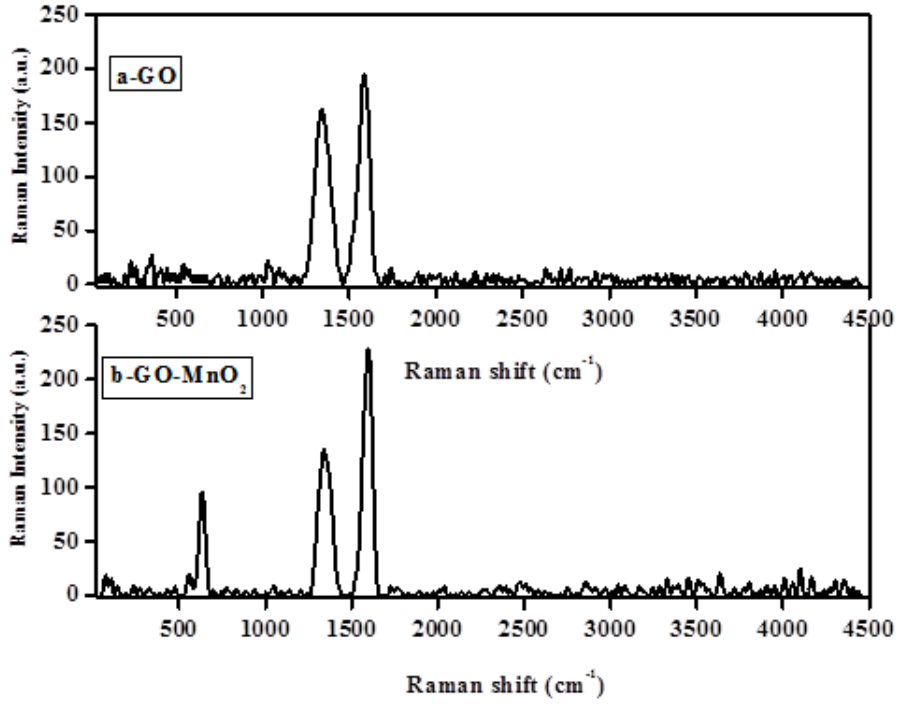

Fig. 5: Raman spectra of the synthesized GO and GO–MnO_2 composite.

Sorption study

The sorption of Eu(III) and Ce(III) ions from aqueous solutions onto the synthesized GO, MnO_2 and GO–MnO_2 composite was carried out using batch technique. The various parameters affecting the sorption of these lanthanides were investigated individually to optimize their sorption on the synthesized samples. The results obtained are discussed in the following sections:

Effect of pH

The solution pH is an important factor affecting both the sorbate and sorbent properties. The effect of pH on sorption of Eu(III) and Ce(III) onto the synthesized samples was carried out at different pH values ranged from 1 up to 7 and the data revealed are given in **Fig. 6**. The plots clarify that sorption of Eu(III) and Ce(III) increases with increasing pH up to ~ 2.5 for Eu(III) and ~ 3 Ce(III). It was observed that at low pH values, sorption of Eu(III) and Ce(III) ions was low which is probably due to protonation of surface active sites and the increase of H_3O^+ ions concentration in aqueous solution. Thus, the competition between H_3O^+ and both Eu(III) and Ce(III) ions for the available binding surface active site decreased Eu(III) and Ce(III) uptake [40]. With increasing the initial pH values, the concentration of H_3O^+ ions decreased and the protonation of the function groups in sorbent surface increased, attaining a negative charge [41]. Hence, the attraction between the surface of the metal ions and the positively charge site in sorbent surface was enhanced. At pH value > 4, the adsorption percentage continuously increased and that could be attributed to the precipitation of REE as hydroxides.

Effect of contact time

The effect of contact time on sorption of Eu(III) and Ce(III) lanthanides onto the surface of the synthesized samples was studied at different agitating times, and the data obtained are represented in **Fig. 7.**

At the initial stage of contact, the sorption rate of Eu(III) and Ce(III) was relatively rapid and the sorption was highly increased with increasing contact time up to 1 h. The sorption of Eu(III) ions by the synthesized GO and GO-MnO_2 composite increased with time till reached equilibrium after ~ 2 h, the sorption extent still constant up to 24 h. In contrast, sorption Eu(II) and Ce(III) onto MnO_2 sorbent was occurred through a relatively low rate and extended up to 24 h to attain equilibrium. Generally, 24 h was considered as a suitable contact time to reach equilibrium in the rest of other experiments.

The sorption of Ce(III) onto GO and GO–MnO_2 composite was slightly increased with time up to 5 h, while 24 h to reach equilibrium in sorption onto MnO_2 sorbent. The uptake percentages of Eu(III) onto the synthesized GO, MnO_2 and GO–MnO_2 composite are 98.03, 75.67 and 98.42 %, respectively. The values 88.94, 74.36, and 91.26 % were recorded for Ce(III) sorption onto the synthesized GO, MnO_2 and GO–MnO_2 composite, respectively. The rapid sorption at initial contact time is related to the availability of a large number of active sites on the adsorbent surface. The plots also clarify that the further increase in contact time beyond 2 and 5 h for sorption of Eu(II) and Ce(III) ions onto GO and GO–MnO_2 composite, and 24 h for their sorption onto MnO_2 particles slightly increased uptake percentages. Generally, an equilibration period of 24 h was selected for all further experiments.

The maximum sorption capacity of synthesized samples for sorption of Eu(III) and Ce(III) ions from aqueous solutions was compared with other sorbents reported in the literature and the data are given in **Table 2**. From the data, it indicates that GO–MnO_2 composite has a high sorption capacity comparing with other adsorbents.

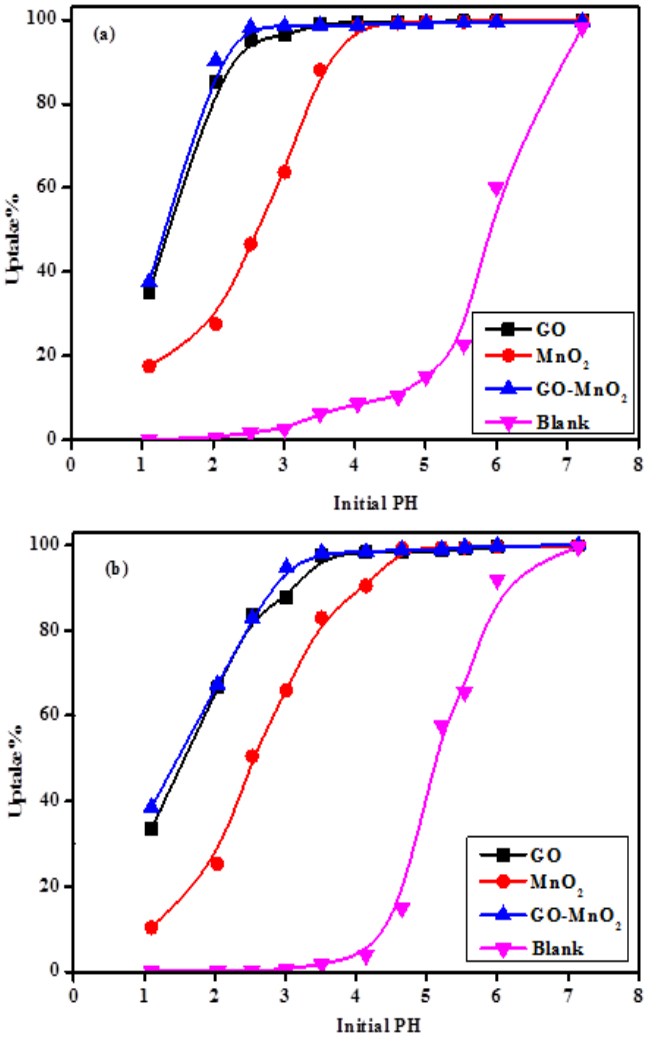

Fig. 6: Effect of initial pH on sorption of a) Eu(III) and b) Ce(III) ions onto synthesized sorbents (C_o = 50 mg.L^{-1}, t_{eq} = 24 h, V/m = 500 mL.g^{-1}).

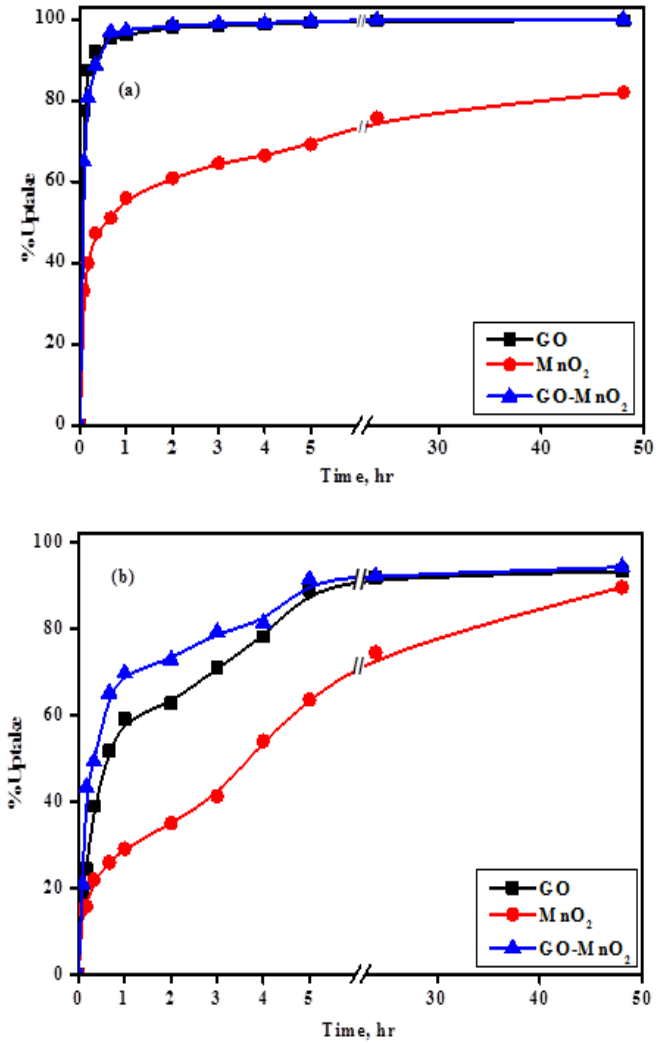

Fig. 7: Effect of contact time on sorption of a) Eu(III) and b) Ce(III) ions onto the synthesized sorbents (C_o = 50 mg.L^{-1}, V/m = 500 mL.g^{-1}, pH = 3.01).

Table 2: Comparison between Eu(III) and Ce(III) sorption capacity with other adsorbents reported in literature

Element	adsorbent	q_{max}(mg/g)	Reference
Eu(III)	GO	81.22	Present work
	MnO_2	70.75	Present work
	GO-MnO_2	103.43	Present work
	Fe_3O_4/GO	70.15	[42]
	Al_2O_3/expanded graphite	5.14	[43]
	(Poly acrylamide-acrylic acid)-Kaolin	54.64	[44]
	Magnetic GMZ bentonite	40.50	[45]
	Natural bentonite	14.9	[46]
Ce(III)	GO	73.5	Present work
	MnO_2	67.11	Present work
	GO-MnO_2	101.71	Present work
	acetylacetone-modified silica gel	19.40	[47]
	Uranium Antimonate	34.4	[48]
	Activated carbon	9.66	[49]
	Cladophora hutchinisia	74.9	[50]

Sorption kinetics

The experimental results were fit to pseudo-first-order and pseudo-second-order models to analyze the sorption kinetics of Eu(III) and Ce(III) ions on the synthesized samples.

A simple pseudo-first-order model was used to correlate the rate of reaction and it was expressed as follow [51]:

$$log(q_e - q_t) = log\ q_e - \frac{k_f}{2.303}t \quad (3)$$

where: q_e and q_t are the amounts of metal ion sorbed on sorbents at equilibrium and time t (mg. g^{-1}), k_f is the pseudo-first-order rate constant (min^{-1}). Plotting the relation of log ($qe - qt$) versus t for sorption of Eu(III) and Ce(III) ions onto synthesized samples gave straight lines. The constants of pseudo-first-order model were graphically estimated, and data are given in **Table 3**.

In addition, Pseudo-second-order model was used to describe sorption kinetics studies using the following equation [52]:

$$\frac{t}{q_t} = \frac{1}{k_s\, q_e^2} + \frac{1}{q_e}t \quad (4)$$

where: q_e and q_t are the amounts of metal ion sorbed on the sorbent at equilibrium and time t (mg. g^{-1}), respectively, k_s is the pseudo-second-order rate constant (g. mg^{-1}. min^{-1}).

The pseudo-second-order constant (K_s) along with the correlation coefficient were graphically determined and are listed in **Table 3.** The obtained results clarify that the correlation coefficient (R^2) is extremely high and closer to unity for pseudo-second-order model compared to that of pseudo-first-order model. Also, the amounts of metal ion sorbed (q_e) determined using pseudo-second-order model are near to the experimental q_e values. This indicates that the kinetic of pseudo-second-order model fit the revealed experimental results. In addition, the sorption of studied REEs on applied sorbents may attained through a chemisorptive process. The rate-determining step in sorption system may be chemical sorption involving valency forces through sharing or exchange of electrons between sorbate and sorbent.

Sorption isotherms

Sorption isotherms express the mathematical relationship between the concentration of a sorbate in liquid phase and its sorption degree onto a sorbent surface at a constant temperature. The experimental data were analyzed using Langmuir and Freundlich isotherm models. Freundlich model was selected to fit the revealed experimental results of Eu(III) and Ce(III) sorption onto synthesized sorbents. The model equation in non- linear form is represented as [53]:

$$q_e = K_F C_e^{\,1/n} \quad (5)$$

where: C_e is the equilibrium concentration of metal in solution ($mg.L^{-1}$), q_e is the amount sorbed of metal ion($mg.g^{-1}$), K_f is Freundlich isotherm constant ($mg^{(1-1/n)}.L^{1/n}.g^{-1}$), 1/n is a Freundlich isotherm exponent constant related to the sorption intensity.

The values of Freundlich isotherm model parameters were determined. These values, in addition to the values of the correlation coefficients (R^2), are given in **Table 4**.

Langmuir model is based on the assumption of monolayer formation of adsorbate ions on the homogeneous adsorbent surface. The model equation in non- linear form is given as [54]:

$$q_e = \frac{q_{max}\, K_L\, C_e}{1 + K_L C_e} \quad (6)$$

where: K_L is Langmuir constant related to the intensity of adsorption ($L.mg^{-1}$) and q_{max} is the maximum adsorbed amount of Eu(III) and Ce(III) ions ($mg.g^{-1}$). The relation C_e and q_e for sorption of Eu(III) and Ce(III) ions onto synthesized samples in non-linear form for Freundlich and Langmuir isotherm models are represented in **Fig. 8&9.** The constants of Langmuir isotherm model were graphically determined and their values along with correlation coefficients (R^2) are listed in **Table 4**.

Comparing the calculated correlation coefficients (R^2) for Freundlich and Langmuir models listed in **Table 4**, it could be concluded that, the correlation coefficients (R^2) of the Langmuir and Freundlich models for the adsorption of Eu(III) and Ce(III) ions on the synthesized GO, MnO_2 and GO–MnO_2 composite are nearer to 0.99. Also, the amounts of metal ion sorbed on sorbents q_e calculated from Langmuir model near to experimental q_e, indicating a better fit with the adsorption Process follows the Langmuir model. This result indicates that the monolayer adsorption of Eu(III) and Ce(III) ions on the synthesized GO, MnO_2 and GO–MnO_2 composite is expected [40].

Sorption thermodynamics

In any sorption process the thermodynamic parameters should be considered to determine what processes will occur spontaneously. The parameters (Gibbs free energy change (ΔG°), enthalpy change (ΔH°) and entropy change (ΔS°) was calculated using the following equation (7):

$$\Delta G^o = -RT\, lnK_d \quad (7)$$

where: R is the ideal gas constant (8.315×10^{-3} $kJ.mol^{-1}.\ K^{-1}$) and T is the absolute temperature in Kelvin (K). Based on changing the distribution constants with temperature, the relation between K_d and the thermodynamic parameters ΔH^o and ΔS^o can be described by Van't Hoff equation [55]:

$$ln\, K_d = \frac{\Delta S^o}{R} - \frac{\Delta H^o}{RT} \quad (8)$$

The relation between ln K_d, 1/T is represented in **Fig. 10.** The values of the parameters ΔH° and ΔS° were graphically estimated from the slopes and intercepts of the linear plots of ln K_d versus 1/T and summarized in **Table 5**. The positive values of ΔH° indicate the endothermic nature of sorption process. The negative ΔG° values indicate the uptake of Eu(III) and Ce(III) ions on synthesized

samples were achieved through a favorably spontaneous process [56]. The positive values of ΔS° also demonstrate the increase in degree of randomness at the solid-liquid interface during sorption of Eu(III) and Ce(III) ions onto the applied samples [57].

Desorption study

Desorption of Eu(III) and Ce(III) ions from loaded synthesized GO, MnO_2 and GO–MnO_2 samples was performed using different organic and inorganic eluents. The used organic eluents were Oxalic, Malonic, Mandelic, Citric, Succinic acids and EDTA, while the inorganic eluents were H_3PO_4, HCl, $MnCl_2$, $FeCl_3$ and $AlCl_3$. The results are shown in **Fig. 11**.

The plots illustrate that Eu(III) and Ce(III) ions were hardly eluted from the adsorbent surface using organic eluents as 0.01 M oxalic acid, 0.001 M Malonic acid, 0.01 M Mandelic acid, 0.01 M Citric acid, 0.01 M Succinic acid. Also, the inorganic eluents 0.001 M H_3PO_4, 0.001 M HCl hardly eluted Eu(III) and Ce(III).

In contrast, both metal ions were easily desorbed with using 0.01 M EDTA, 0.01 M $AlCl_3$, 0.1 M $FeCl_3$ and 0.1 M $MnCl_2$ solutions. The percentages of Eu(III) eluted from GO were 90.98, 88.99, 83.80 and 29.04 % with using 0.01 M EDTA, 0.01 M $AlCl_3$, 0.1 M $FeCl_3$ and 0.1 M $MnCl_2$, respectively. The amounts of Eu(III) eluted from MnO_2 using the previously mentioned eluents were 75.08, 58.85, 71.94 and 21.35 %, respectively.

Also, the amounts of Eu(III) eluted from GO–MnO_2 composite using the same eluents were 90.51, 23.08, 73.52 and 13.33 %, respectively. The percentages of Ce(III) eluted from GO using the previously mentioned eluents were 97.21, 59.86, 98.90 and 58.02 %, respectively. The amounts of Ce(III) eluted from MnO_2 using the previously mentioned eluents were 43.96, 81.31, 85.58 and 51.43 %, respectively. Finally, the amounts of Ce(III) eluted from GO–MnO_2 composite using the previously mentioned eluents were 46.92, 98.55, 97.22 and 39.46 %, respectively. This may be to ion exchange of Al(III), Fe(III) and Mn(II) with Eu(III) and Ce(III) ions. The amounts of Ce(III) eluted from GO, MnO_2 and GO–MnO_2 composite using 0.01 M citric acid were 22.35, 36.55 and 24.85 %, respectively. On other hand, this eluent has no effect on desorption of Eu(III) ions from these sorbents. From these data Eu(III) ions were easily eluted with 0.01 M EDTA than Ce(III) due to EDTA form complex with Eu(III) with stability constant 17.35 higher than Ce(III) in which EDTA form complex with Ce(III) with stability constant 15.98. Also, Ce(III) ions were easily eluted with 0.01 M $AlCl_3$ than Eu(III) due to ionic radius of Ce(III) (1.03 A°) is higher than ionic radius of Eu(III) (0.95 A°) and easily exchanged with Al(III) which has low ionic radius(0.53 A°). This variation in desorption percentages may be referred to the involved sorption mechanism and the physico-chemical properties of these sorbents.

Table 3: Kinetic parameters and correlation coefficients (R^2) of pseudo-first-order and pseudo-second-order kinetic models for Eu(III) and Ce(III) sorption on the synthesized sorbents

Kinetic parameters		Element					
		Eu(III)			Ce(III)		
Model	Parameters	GO	MnO_2	GO-MnO_2	GO	MnO_2	GO-MnO_2
Pseudo-first order	K_f (min^{-1})	0.011	0.004	0.012	0.008	0.003	0.008
	q_e (mg. g^{-1})	2.745	9.829	3.299	13.75	18.98	17.33
	R^2	0.889	0.906	0.784	0.868	0.949	0.903
	S.D.	6.24×10^{-4}	1.99×10^{-4}	9.53×10^{-4}	4.92×10^{-4}	1.14×10^{-4}	3.93×10^{-4}
Pseudo-second order	k_s (g.mg^{-1}.min^{-1})	0.023	0.004	0.017	0.003	0.001	0.002
	h (mg. g^{-1}.min^{-1})	14.43	1.50	10. 927	1.4	0.298	0. 911
	q_e (mg. g^{-1})	24.894	17.547	25.05	21.83	16.2127	20.99
	R^2	0.999	0.997	0.999	0.998	0.998	0.999
	S.D.	6.23×10^{-5}	9.96×10^{-4}	6.98×10^{-5}	7.25×10^{-4}	1.02×10^{-3}	4.82×10^{-4}

Table 4: Freundlich and Langmuir isotherms constants for Eu(III) and Ce(III) ions sorption onto the synthesized sorbents

Model	Parameters	Element					
		Eu(III)			Ce(III)		
		GO	MnO_2	GO-MnO_2	GO	MnO_2	GO-MnO_2
Freundlich constants	k_F	41.95	6.37	48.49	19.52	4.33	19.17
	$1/n$	0.244	0.394	0.239	0.251	0.522	0.291
	SD	0.462	0.135	0.408	0.422	0.121	0.282
	R^2	0.941	0.986	0.952	0.961	0.983	0.974
Langmuir constants	Q_{max}	108.74	58.24	113.41	66.82	87.32	80.72
	k_L	0.392	3330.023	0.674	0.113	0.013	0.081
	SD	0.053	0.003	0.001	0.023	0.001	0.013
	R^2	0.981	0.989	0.975	0.961	0.993	0.974

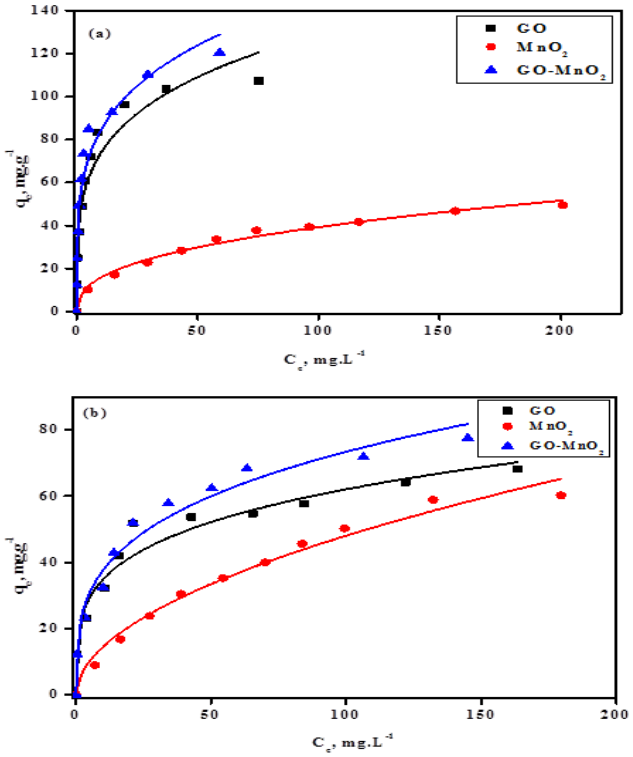

Fig. 8: Freundlich isotherm plots for sorption of a) Eu(III) and b) Ce(III) ions onto synthesized sorbents (pH = 3.01, t_{eq} = 24 h, V/m = 500 mL.g^{-1}).

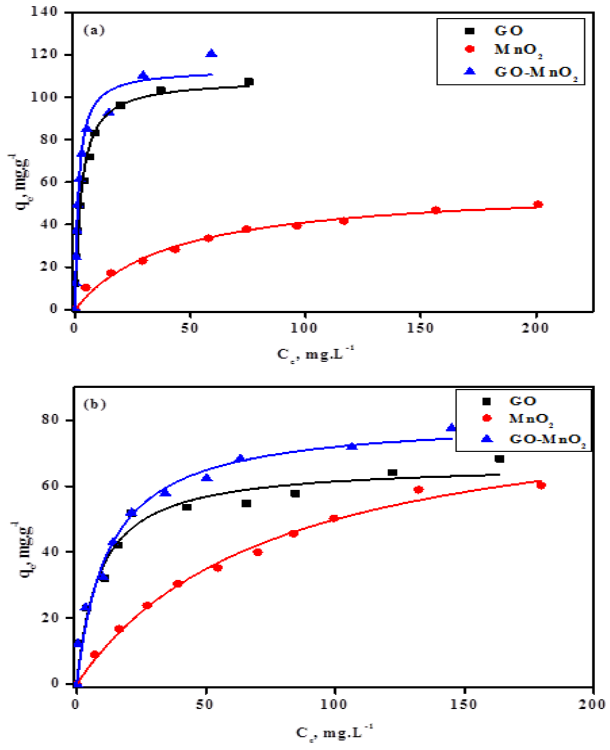

Fig. 9: Langmuir isotherm plots for sorption of a) Eu(III) and b) Ce(III) ions onto synthesized sorbents (pH = 3.01, t_{eq} = 24 h, V/m = 500 mL.g^{-1}).

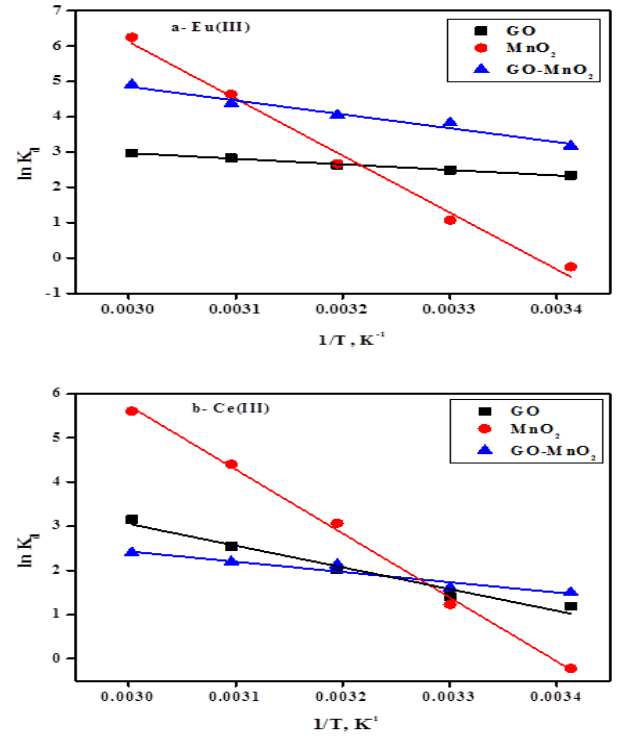

Fig.10: Van't Hoff plot for sorption of a) Eu(III) and b) Ce(III) ions onto synthesized sorbents (C_o = 50 mg.L^{-1},V/m = 500 mL.g^{-1}, t_{eq} = 24 h, pH = 3.01).

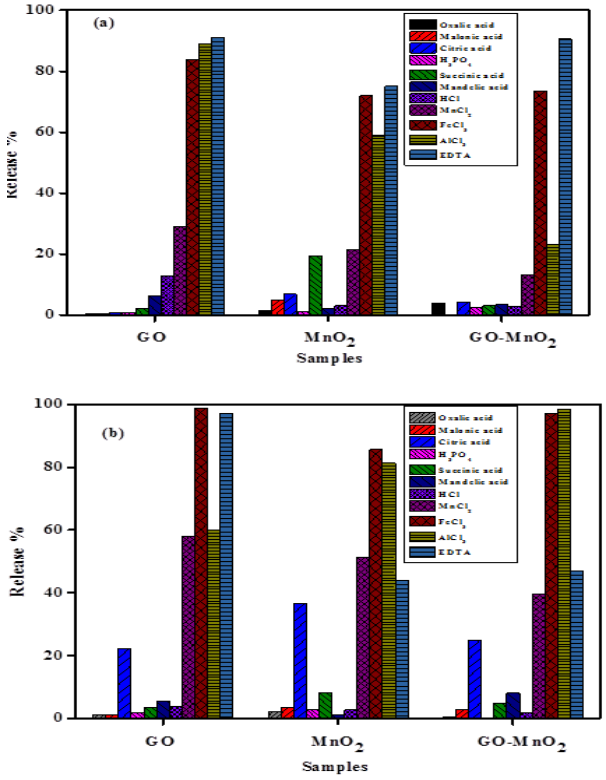

Fig. 11: Effect of different eluents on desorption of a) Eu(III) and b) Ce(III) ions from synthesized sorbents (C_o = 50 mg.L^{-1}, t_{eq} = 24 h, V/m = 500 mL.g^{-1}, pH = 3.01).

Table 5: Thermodynamic parameters for for Eu(III) and Ce(III) ions sorption onto the synthesized sorbents

Element	Sorbents	Thermodynamic parameters			
		Temperature (°C)	ΔG°- (kJ.mol^{-1})	ΔS° (kJ.mol^{-1}.K^{-1})	ΔH° (kJ.mol^{-1})
Eu(III)	GO	20	5.642	0.064	13.119
		30	6.282		
		40	6.923		
		50	7.563		
		60	8.203		
	MnO_2	20	1.300	0.453	133. 956
		30	3.227		
		40	7.754		
		50	12.282		
		60	16.809		
	GO-MnO_2	20	7.874	0.138	32.753
		30	9.255		
		40	10.635		
		50	12.016		
		60	13.396		
Ce(III)	GO	20	2.468	0.148	40.919
		30	3.967		
		40	5.449		
		50	6.931		
		60	8.412		
	MnO_2	20	0.607	0.409	120.437
		30	3.483		
		40	7.572		
		50	11.662		
		60	15.752		
	GO-MnO_2	20	3.580	0.078	19.327
		30	4.362		
		40	5.144		
		50	5.926		
		60	6.708		

Conclusion

In this study, GO, MnO_2 and GO–MnO_2 composite were synthesized and applied as sorbents for some rare earth elements. Sorption of Eu(III) and Ce(III) ions from aqueous solutions have been carried out using batch technique. The sorption behavior of Eu(III) and Ce(III) ions at different experimental conditions has been examined and the results obtained show that sorption process is dependent on pH value. The maximum sorption capacity of GO was 81.22 and 73.50 mg/g for Eu(III) and Ce(III), respectively, and sorption capacity of MnO_2 was 70.75 and 67.11 mg/g for Eu(III) and Ce(III), respectively, and sorption capacity of GO–MnO_2 composite was 103.43 and 101.71 mg/g for Eu(III) and Ce(III), respectively. The sorption processes of Eu(III) and Ce(III) ions onto synthesized GO, MnO_2 and GO–MnO_2 composite follows pseudo second-order kinetics and Langmuir models.

Thermodynamically, sorption process is spontaneous and endothermic in nature. The results suggest that GO–MnO_2 composite have great potential to be used as economical and efficient adsorbents for lanthanides sorption from aqueous solutions. MnO_2 coated on GO surface using a simple method improves the mechanical properties of GO consequently GO easily separated during adsorption experiments may provide ideas for modifying other materials.

References

1) **Metwally, S. S. and Rizk, H. E. (2014).** Preparation and characterization of nano-sized iron–titanium mixed oxide for removal of some lanthanides from aqueous solution. Sep. Sci. Technol., **49:** 2426-2436.
2) **Kapnisti, M. G., Noli, F. G., Papastergiadis, E. S. and Pavlidou, E. G. (2018).** Exploration of the parameters affecting the europium removal from aqueous solutions by novel synthesized titanium phosphates. J. Environ. Chem. Eng., **6:** 3408-3417.
3) **Fryxell, G. F., Chouyyok, W. and Rutledge, R. D. (2011).** Design and synthesis of chelating diamide sorbents for the separation of lanthanides. Inorg. Chem. Commun., **14:** 971–974.
4) **Krishnamurthy, N. and Gupta, C. K. (2015)**. Extractive metallurgy of rare earths CRC Press, Boca Raton, FL.

5) **Murthy, Z. V. P. and Choudhary**, **A. (2011)**. Separation of cerium from feed solution by nanofiltration. Desalination, **279** (1): 428–432.
6) **Zhu, X. and Alexandratos**, **D. S. (2015)**. Development of a new ion exchange coordinating phosphate ligand for the sorption of U(VI) and trivalent ions from phosphoric acid solutions. Chem. Eng. Sci., **127:** 126-132.
7) **Chen, Z., Wang, W., Sang, F., Xu, J., Luo, G. and Wang**, **Y. (2017)**. Fast extraction and enrichment of rare earth elements from waste water via microfluidic-based hollow droplet. Sep. Purif. Technol., **174:** 352-361.
8) **Wannachod, T., Leepipatpiboon, N., Pancharoen, U. and Nootong**, **K. (2014).** Separation and mass transport of Nd(III) from mixed rare earths via hollow fiber supported liquid membrane: experiment and modeling. Chem. Eng. J., **248:** 158–167.
9) **Yakout, S. M., Metwally, S. S. and El-Zakla, T. (2013)**. Uranium sorption onto activated carbon prepared from rice straw: competition with humic acids. Appl. Surf. Sci., **280:** 745-750.
10) **Veliscek-Carolan, J., Jolliffe, K. and Hanley, T. (2013).** Selective sorption of actinides by titania nanoparticles covalently functionalized with simple organic ligands. ACS Appl. Mater. Interfaces., **5:** 11984-11994.
11) **Xu, P., Zeng, G. M., Huang, D. L., Feng, C. L., Hu, S., Zhao, M. H., Lai, C., Wei, Z., Huang, C., Xie, G. X. and Liu, Z. F. (2012).** Use of iron oxide nanomaterials in wastewater treatment: a review. Sci. Total Environ., **424:** 1–10.
12) **Zhao, G., Li, J., Ren, X., Chen, C. and Wang, X. (2011).** Few-layered graphene oxide nanosheets as superior sorbents for heavy metal ion pollution management. Environ. Sci. Technol., **45:** 10454-10462.
13) **Sun, Y., Wang, Q., Chen, C., Tan, X. and Wang, X. (2012).** Interaction between Eu(III) and graphene oxide nanosheets investigated by batch and extended X-ray absorption fine structure spectroscopy and by modeling techniques. Environ. Sci. Technol., **46:** 6020-6027.
14) **Zhao, G. H., Ren, X. M., Gao, X., Tan, X. L., Li, J. X., Chen, C. L., Huang, Y. Y. and Wang, X. K. (2011).** Removal of Pb(II) ions from aqueous solutions on few-layered graphene oxide nanosheets. Dalton Trans., **40:** 10945-10952.
15) **Sheng, G. D., Yang, S. T., Li, Y. M., Gao, X., Huang, Y. Y., Hu, J. and Wang, X. K. (2014).** Retention mechanisms and microstructure of Eu(III) on manganese dioxide studied by batch and high resolution EXAFS technique. Radiochim. Acta, **102** (1–2): 155-167.
16) **Varga, Z. (2007).** Preparation and characterization of manganese dioxide impregnated resin for radionuclide pre-concentration. Appl. Radiat. Isotopes, **65:** 1095-1100.
17) **Fairhurst, A. J., Warwick, P. and Richardson, S. (1995).** The influence of humic acid on the adsorption of europium onto inorganic colloids as a function of PH. Colloids Surf., A: Physicochem. Eng. Aspects, **99:** 187-199.
18) **Sumboja, A., Foo, C. Y., Wang, X. and Lee, P. S. (2013).** Large areal mass, flexible and free-standing reduced graphene oxide/manganese dioxide paper for asymmetric supercapacitor device. Adv. Mater., **25:** 2809-2815.
19) **Pan, N., Li, L., Ding, J., Li, S., Wang, R., Wang, X., Xia, C. and Jin, J. (2016).** Preparation of graphene oxide-manganese dioxide for highly efficient adsorption and separation of Th(IV)/U(VI). J. Hazard. Mater., **309:** 107-115.
20) **Zhao, G. X., Li, J. X., Ren, X. M., Chen, C. L. and Wang, X. K. (2011).** Few layered graphene oxide nanosheets as superior sorbents for heavy metal ion pollution management. Environ. Sci. Technol., **45:** 10454-10462.
21) **Subramanian, V., Zhu, H. and Wei**, **B. (2008)**. Alcohol-assisted room temperature synthesis of different nanostructured manganese oxides and their pseudo capacitance properties in neutral electrolyte. Chem. Phys. Letters, **453:** 242-249.
22) **Gan, T., Sun, J., Huang, K., Song, L. and Li**, **Y. (2013)**. A graphene oxide–mesoporous MnO_2 nanocomposite modified glassy carbon electrode as a novel and efficient voltammetric sensor for simultaneous determination of hydroquinone and catechol. Sens. Actuators, B., **177:** 412-418.
23) **Chandra, V., Park, J., Chun, Y., Lee, J. W., Hwang, I. C. and Kim, K. S. (2010)**. Water-dispersible magnetite-reduced graphene oxide composites for arsenic removal. ACS Nano., **4:** 3979-3986.
24) **Fei, Y., Yong, L., Sheng, H. and Jie**, **M. (2016)**. Adsorptive removal of ciprofloxacin by sodium alginate/graphene oxide composite beads from aqueous solution. J. Colloid Interface Sci., **484:** 196-204.
25) **Wang, H., Yuan, X., Wu, Y., Huang, H., Zeng, G., Liu, Y., Wang, X., Lin, N. and Qi**, **Y. (2013)**. Adsorption characteristics and behaviors of graphene oxide for Zn(II) removal from aqueous solution. Appl. Surf. Sci., **279:** 432-440.
26) **Luo, X., Wang, C., Luo, S., Dong, R., Tu, X. and Zeng, G. (2012).** Adsorption of As(III) and As(V) from water using magnetite Fe_3O_4-reduced graphite oxide–MnO_2 nanocomposites. Chem. Eng. J., **187:** 45-52.
27) **Parida, K. M., Mallick, S., Mohapatra, B. K. and Misra**, **N. V. (2004).** Studies on manganese-nodule leached residues: Physicochemical characterization and its adsorption behavior toward Ni^{2+} in aqueous system. J. Colloid Interface Sci., **277:** 48–54.
28) **Ren, Y., Yan, N., Feng, J., Ma, J., Wen, Q., Li, N. and Dong**, **Q. (2012)**. Adsorption mechanism of copper and lead ions onto graphene nanosheet/δ-MnO_2. Mater. Chem. and Phys., **136:** 538–544.
29) **Song, W., Wang, X., Wang, Q., Shao, D. and Wang**, **X. (2015)**. Plasma-induced grafting of polyacrylamide on graphene oxide nanosheets for simultaneous removal of radionuclides. Phys. Chem. Chem. Phys., **17:** 398-406.
30) **Zhang, J., Jiang, J. and Zhao**, **X. S. (2011)**. Synthesis and capacitive properties of manganese oxide nanosheets dispersed on functionalized graphene sheets. J. Phys. Chem. C, **115:** 6448-6454.

31) **Zhang, X., Yu, P., Zhang, H., Zhang, D., Sun, Z. and Ma**, **Y. (2013)**. Rapid hydrothermal synthesis of hierarchical nanostructures assembled from ultrathin birnessite-type MnO_2 nanosheets for supercapacitor applications. Electrochim. Acta, **89:** 523-529.

32) **Zhang, Y., Su, M., Ge, L., Ge, S., Yu, J. and Song**, **X. (2013)**. Synthesis and characterization of graphene nanosheets attached to spiky MnO_2 nanospheres and its application in ultrasensitive immunoassay. Carbon, **57:** 22-33.

33) **Nakajima, T., Mabuchi, A. and Hagiwara, R. (1988)**. A new structure model of graphite oxide. Carbon, **26:** 357–361.

34) **Liu, Y., Yan, D., Zhuo, R., Li, S., Wu, Z., Wang, J. and Geng**, **Z. (2013)**. Design, hydrothermal synthesis and electrochemical properties of porous birnessite-type manganese dioxide nanosheets on graphene as a hybrid material for supercapacitors. J. Power Sourc., **242:** 78–85.

35) **Vimuna, V. M., Athira, A. R. and Xavier, T. S. (2018)**. Microwave assisted synthesis of graphene oxide-MnO_2 nanocomposites for electrochemical supercapacitors. Appl. Phys. Lett., **1953:** 1-4.

36) **Xu, C., Wang, X. and Zhu**, **J. (2008).** Graphene-metal particle nanocomposites. J. Phys. Chem. C., **112:** 19841-19845.

37) **Kudin, K. N., Ozbas, B., Schniepp, H. C., Prud'homme, R. K., Aksay, I. A. and Car, R. (2008)**. Raman spectra of graphite oxide and functionalized graphene sheets. Nano Lett., **8:** 36-41.

38) **Ni, Z. H., Wang, Y. Y., Yu, T. and Shen**, **Z. X. (2008)**. Raman spectroscopy and imaging of graphene. Nano Res., **1:** 273–291.

39) **Sreeprasad, T. S., Shihabudheen M. M., Lisha, K. P. and Pradeep**, **T. (2011).** Reduced graphene oxide–metal/metal oxide composites: Facile synthesis and application in water purification. J. Hazard. Mater., **186:** 921-931.

40) **Luo, C., Wei, R., Guo, D., Zhang, S. and Yan**, **S. (2013)**. Adsorption behavior of MnO_2 functionalized multi-walled carbon nanotubes for the removal of cadmium from aqueous solutions. Chem. Eng. J., **225:** 406-415.

41) **Ren, X., Chen, C., Nagatsu, M. and Wang**, **X. (2011).** Carbon nanotubes as adsorbents in environmental pollution management: a review. Chem. Eng. J., **170:** 395–410.

42) **Li, D., Zhang, B. and Xuan, F. (2015).** The sorption of Eu(III) from aqueous solutions by magnetic grapheme oxides: A combined experimental and modeling studies. J. Mol. Liq., **211:** 203–209.

43) **Li, D., Zhang, B. and Xuan, F. (2015).** The sorption of Eu(III) from aqueous solutions by magnetic grapheme oxides: A combined experimental and modeling studies. J. Mol. Liq., **211:** 203–209.

44) **Sun, Y., Chen, C., Tan, X., Shao, D., Li, J., Zhao, G., Yang, S., Wang, Q. and Wang, X. (2012).** Enhanced adsorption of Eu(III) on mesoporous Al2O3/expanded graphite composites investigated by macroscopic and microscopic techniques. Dalton Trans., **41:** 13388-13394.

45) **Metwally, S. S., Hassan, R. S., El-Masry, E. H. and Borai**, **E. H. (2017)**. Gamma-induced radiation polymerization of kaolin composite for sorption of lanthanum, europium and uranium ions from lowgrade monazite leachate. J. Radioanal. Nucl. Chem., **315:** 1-11.

46) **Chen, Y., Zhu, B., Wu, D., Wang, Q., Yangc, Y., Ye, W. and Guo**, **J. (2012)**. Eu(III) adsorption using di(2-thylhexly) phosphoric acid-immobilized magnetic GMZ bentonite. Chem. Eng. J., **181:** 387–396.

47) **Ralf, K. and Horst**, **B. P. (2010)**. Influence of geochemical parameters on the sorption and desorption behavior of europium and gadolinium onto kaolinite. J. Environ. Monit., **12:** 1295-1301.

48) **Zhang, N., Huang, C. and Hu**, **B. (2007).** ICP-AES determination of trace rare earth elements in environmental and Food samples by on-line separation and preconcentration with acetylacetone-modified silica gel Using microcolumn. Anal. Sci., **23:** 997–1002.

49) **Sivaiah, M. V., Venkatesan, K. A., Sasidhar, P., Krishna, R. M. and Murthy**, **G. S. (2004)**. Ion exchange studies of cerium(III) on uranium antimonate. J. Nucl. Radiochem. Sci., **5:** 7-10.

50) **Mahmoud, M. R., El-deen, G. E. S. and Soliman**, **M. A. (2014)**. Surfactant-impregnated activated carbon for enhanced adsorptive removal of Ce(IV) radionuclides from aqueous solutions. Ann. Nucl. Energy, **72:** 134-144.

51) **Torab-Mostaedi, M., Asadollahzadeh, M., Hemmati, A. and Khosravi**, **A. (2015)**. Biosorption of lanthanum and cerium from aqueous solutions by grapefruit peel: equilibrium, kinetic and thermodynamic studies. Res. Chem. Intermed., **41:** 559–573.

52) **Lagergren, S. (1898)**. About the theory of so-called adsorption of soluble substances. Kongl. Sv. vet. akademiens handlingar, **24:** 1–39.

53) **Ho, Y. S. and McKay**, **G. (1999)**. Pseudo-second order model for sorption processes. Proc. Biochem., **34:** 451–465.

54) **Freundlich**, **H. M. F. (1906)**. Over the adsorption in solution. J. Phys. Chem., **57:** 385-471.

55) **Langmuir**, **L. (1918).** Adsoption of gases on plane surfaces of glass, mica and platinum. J. Am. Chem. Soc., **40:** 1361–1403.

56) **Kolodynska**, **D. (2010)**. The effect of the novel complexing agent in removal of heavy metal ions from waters and waste waters. Chem. Eng. J., **165:** 835-845.

57) **Wang, Q., Chen, L. and Sun**, **Y. B. (2012)**. Removal of radiocobalt from aqueous solution by oxidized MWCNT. J. Radioanal. Nucl. Chem., **291:** 787–795.

58) **Ding, C. C., Cheng, W. C., Sun, Y. B. and Wang**, **X. K. (2015)**. Effects of *Bacillus subtilis* on the reduction of U(VI) by nano-Fe^0. Geochim. Cosmochim. Acta., **165:** 86–107.